COMPARISON OF OPTIMAL SMALL SPACECRAFT MICRO ELECTRIC PROPULSION TECHNOLOGIES FOR MISSION OPPORTUNITIES

Sara Spangelo
Jet Propulsion Laboratory, California Institute of Technology
4800 Oak Grove Drive, Pasadena, CA 91109; 1-818-354-0699
Sara.Spangelo@jpl.nasa.gov

ABSTRACT

The goal of this paper is to explore the mission opportunities that are uniquely enabled by U-class Solar Electric Propulsion (SEP) technologies. Small SEP thrusters offers significant advantages relative to existing technologies and will revolutionize the class of mission architectures that small spacecraft can accomplish by enabling trajectory maneuvers with significant ΔV requirements and reaction wheel-free attitude control. This paper aims to develop and apply a common system-level modeling framework to evaluate these thrusters for relevant upcoming mission scenarios, taking into account the mass, power, volume, and operational constraints of small highly-constrained missions. We will identify the optimal technology for broad classes of mission applications for different U-class spacecraft sizes and provide insights into what constrains the system performance to identify technology areas where improvements are needed.

INTRODUCTION

Motivation

Recent technology advancements in miniaturized propulsion systems, such as Busek's thrusters, MIT's ion Electrospray Propulsion System (iEPS), Clyde Space's CubeSat Pulse Plasma Thruster, Michigan/Aether's CubeSat Ambipolar Thruster (CAT), and JPL's Micro Electrospray Propulsion (MEP) thruster [1], are being developed that satisfy the size, power, thermal, and launch constraints of small spacecraft, in particular U-class systems. Small spacecraft with MEP will be capable of forming and maintaining Earth imaging constellations, drag make-up, formation flying, proximity operations, hovering (over comets, asteroids, or in Earth orbit), and precision pointing missions in both Earth orbit and interplanetary destinations. This will be a game-changer because for the first time small spacecraft will be able to form and maintain large apertures, accomplish SMEX or Discovery-class science, explore dangerous and unexplored regions of the solar system like Earth-Sun L4/L5, comets, or moons like Europa as precursor missions for a fraction of the cost of conventional mission architectures.

This is an exciting time for small SEP thrusters due to the considerable CubeSat flight heritage in LEO as well as the upcoming mission opportunities for CubeSats to operate and perform ambitious science and technology goals beyond Earth orbit, such as for planetary [2], astrophysics, and heliophysics applications. Flying small SEP thrusters is enabled by considerable advances in telecommunication and navigation, high accuracy attitude determination and control systems, high-efficiency body-fixed and deployable solar arrays, and the emergence of integrated bus architectures and radiation-tolerant U-class components.

There is a large body of work studying a variety of large and small spacecraft thrusters, as well as systems-level approaches to study the applicability of thrusters for existing missions subject to small spacecraft constraints. Solar electric propulsion (SEP) has been proposed and used on a variety of interplanetary mission architectures on large missions, including optimized trajectories to the Mars surface for scientific exploration, Discovery-class mission applications, and asteroid belt missions [3, 4, 5, 6, 7, 8]. Recent work has demonstrated the applicability of electric propulsion solutions for optimal time and propellant solutions for operational responsiveness in LEO [9]. Similar systems-level studies have optimized CubeSat missions with SEP for Earth-escape trajectories [10], and optimized thrusters for representative mission applications [11], which inform our approach. The feasibility of using the Miniature Xenon Ion (MiXI) thruster for a lunar CubeSat mission was investigated, including power, thermal, and bus subsystem sizing [12]. However, there is currently no work in the literature comparing the performance of existing and emerging small spacecraft thruster technologies for relevant mission applications

using a system-level approach. Most of the work has focused on optimizing a single thruster for a single or handful of mission applications, and the performance metrics often differ.

The results of this study will help inform mission formulators, architects, system engineers, and researchers about the best thrusters for their applications. They will also inform technologists which thruster properties have the greatest impact on performance in the context of realistic missions and spacecraft constraints. We also hope to inform future proposal calls about the potential to accomplish novel science investigations or replace SMEX or Discovery-class missions and perform high ΔV Earth and interplanetary orbit transfers with small spacecraft form-factors.

MODEL

We expand our existing systems-level integrated spacecraft models and integrated simulation environment to enable end-to-end simulation and optimization of missions. The environment includes analytic representations of power, structure, thermal, telecommunication, attitude control, propulsion subsystems; orbit and attitude dynamics; and environmental factors. We integrate the vehicle and mission trajectory/attitude optimization problems to enhance overall mission performance and robustness.

We model the expected performance of emerging thruster technologies in this environment, described in Table 1. We optimize mission performance by exploring Pareto trade-offs between objectives such as maximizing payload mass fraction and minimizing orbit transfer times or required thruster lifetimes. We include decisions such as the number of thrusters; thrust strategies for the classes of mission applications; and constraints on mass, volume, power, and performance of state-of-the-art CubeSat components.

Throughout the analysis, we use the CubeSat form-factor, where a 1U = 10 cm x 10 cm x 10 cm with a mass less than 2 kg as the scaling metric for spacecraft. In this paper we explore applicability of small SEP technologies for a range of small spacecraft flight demonstration platforms (e.g. dedicated 3-12U CubeSats). A detailed set of modeling assumptions, scaling laws, and parameters are provided in Ref. [11], which we only summarize at a high level here.

Modeling Framework

The multi-disciplinary system-level modeling approach is demonstrated in Fig. 1, where we flow through this process for ever scenario and spacecraft size/mass we're interested in studying. First, the trajectories are defined in terms of specific impulse (I_{sp}), thrust, power ratios, mass ratios. The trajectories are defined using orbital analysis tools or defining a required Δ V to perform a certain maneuver. Second, we size the propulsion system by determining the number of required thrusters and their power level to deliver the needed thrust that can be accommodated within the spacecraft. We assume that at minimum the spacecraft must accommodate one of the thruster units in Table 1 due to the difficulty in scaling several of the technologies to even smaller systems. However, we also assume that a fractional number of thrusters greater than one may be used, which represents a scaled system or different operating point. For a given spacecraft size (e.g. 6U CubeSat) we assume the maximum allowable mass, M_{max}, and compute the required propellant mass. We assume 10% of the propellant mass is additionally required for the propellant tank. Third we size the solar panels and check the feasibility of the power and thermal systems given our scaling relationships as in Fig. 2. Fourth the spacecraft mass, M_{sc} is computed as the sum of the propulsion system mass (thruster, propellant, tank), M_{prop}, the bus mass (ADCS, EPS, radio, structure, etc.), M_{prop}, and the solar panel mass, M_{sp} as in Eq. 1.

$$M_{sc} = M_{prop} + M_{bus} + M_{sp} \tag{1}$$

$$M_m = \frac{M_{max} - M_s c}{M_{max}} \cdot 100\% \tag{2}$$

Fifth and finally, the mass margin, M_m, is computed as the percentage of the remaining mass relative to the maximum allowable mass for that spacecraft size, M_{max} as in Eq. 2.

Solutions that are found to be infeasible, in particular can not be accommodated within the spacecraft size due to mass, power, solar panel or radiator area, or volume constraints will be removed from the set of candidate solutions. Our modeling code rapidly explores this space for dozens of design points and delivers Pareto fronts showing the trade-offs between performance metrics.

SPACECRAFT AND THRUSTERS OVERVIEW

Spacecraft Design and Scaling

For the spacecraft bus, we selected the Blue Canyon XB1 bus as it represents the state-of-the art and is being utilized for a variety of LEO and interplanetary applications [13]. The XB1 includes most major CubeSat subsystems including a Guidance, Navigation, and Control (GNC) system, Command and Data Handling (CDH) system, and Electric Power System (EPS). The active attitude determination and control system (ADCS) is required to achieve the desired

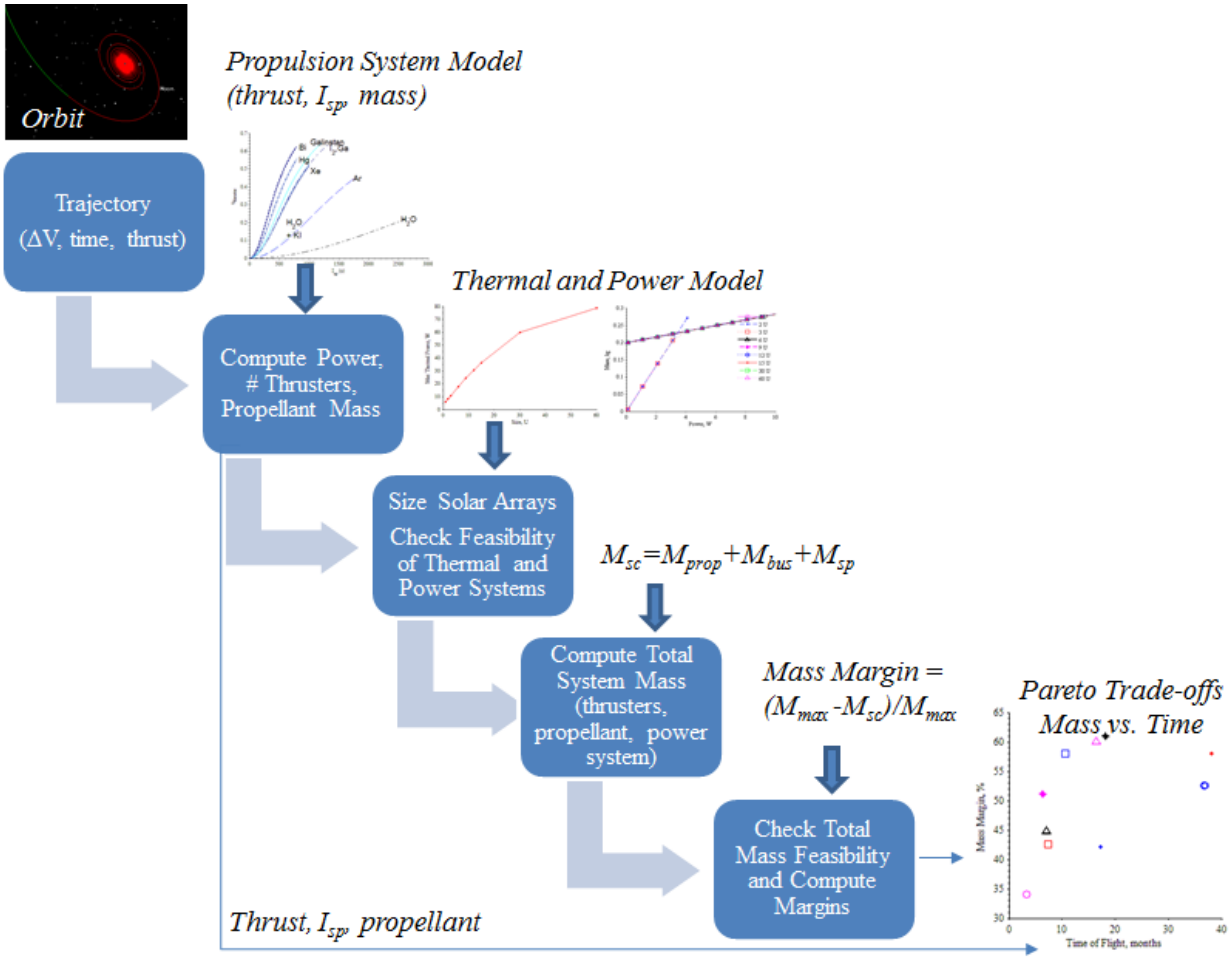

Figure 1: Modeling architecture to generate Pareto trade-offs for mission scenarios

Table 1: Single thruster parameters for emerging small SEP technologies

Thruster Name	Technology	System Input Power	Thrust	I_{sp}	System Mass	System Volume
	Units	W	mN	sec	kg	U
MIT iEPS	Electrospray	50	2.28	2000	0.1	1
JPL's MEP	Electrospray	8.16	0.174	3744	0.16	.04
Busek's 0.1mN MEP	Electrospray	5.5	0.1	2300	0.35	0.26
Busek's 0.7mN MEP	Electrospray	15	0.7	800	1.15	0.33
Busek's Ion (BIT-1)	Hall Effect	13	0.1	2150	0.053	1
Busek's Ion (BIT-3)	Hall Effect	75	1.4	3500	0.2	0.45
CAT Plasma	Magnetoplasma	125	10	1010	0.5	0.1
MiXI Ion	Ion	50	1.5	3000	0.25	1

thrust vector throughout any orientation. The XB1 ADCS consists of a reaction wheel assembly (RWA), internal measurement unit, magnetometer, torque rods, sun sensors, star trackers, and GPS. The XB1 system is currently developed to operate in LEO, is being designed for extended missions in interplanetary locations. Conventional de-saturation techniques are not feasible for interplanetary spacecraft, for example magnetometers can not be used for reaction wheel de-saturation as conventionally done in LEO environments. For missions beyond LEO, reaction wheel saturation is dominated by solar pressure and careful control of solar panel orientation can overcome this challenge. The Blue Canyon bus contains a battery with an energy storage of 25 Whr. The BCT XB1 system nominally has a mass of about 1200 grams, without a RWA. The RWA

is sized based on the momentum, which is a function of the CubeSat mass, where the RWA mass is a cubic function of spacecraft mass based on a curve fit from BCT wheels [11]. The Aluminum structure is assumed to weigh 100 grams per CubeSat U (10 cm x 10 cm x 10 cm), or $M_{max} = 100$ grams/U.

For near-Earth applications, we assume use of an S-Band or UHF transceiver, which has a mass of 80 grams. Existing UHF, S-Band, and X-Band systems do not currently have the capability to return data at meaningful rates to Earth on small spacecraft form-factors. For applications beyond LEO, such as those that escape Earth orbit and operate in deep space, we assume use of the Iris transponder, which is used for both tracking and navigation. The Iris transponder is a low mass (500 grams), volume, and power solution for interplanetary small spacecraft, which communicates to the Deep Space Network (DSN) on X-Band frequencies.
Consistent with the CubeSat design philosophy we've selected Commercial Off-The-Shelf (COTS) components for a low mass and cost design, where many components have flight heritage in LEO. The detailed solar panel and radiation scaling laws that represent U-class spacecraft are provided in Ref. [11]. The solar panel maximum power values are shown in Fig.2, where deployed panels are assumed to track the Sun and the power of the body-fixed panels is scaled according to expected average Sun angles. The maximum surface area available for each CubeSat size and the resultant maximum heat load is shown in Fig. 2b. The fraction of thruster system input power that returns to the bus as heat depends on the thruster, see Table 1. We assume that only this heat needs to be rejected by the radiator. For spacecraft that are 3U or larger where deployable solar panels are an option, the thermal system limits the allowable operating power.

Thrusters

The various thrusters are shown in Table 1, where we've selected only thrusters that could fit and function within a 3U CubeSat. These values represent the system-level power, mass, and volume, including the thruster, Power Processing Unit (PPU), electronics, and feed system where appropriate. In particular, the power values given are the power into the PPU, accounting for its inefficiencies. We assume the thruster controller is part of the spacecraft bus and not included in these numbers. The diversity in I_{sp} and thrust levels are clear from these options, as well as the thruster masses and volumes. Note that these are only single operating points for each of the thrusters based on publicly available data and the thrusters have an operational range.

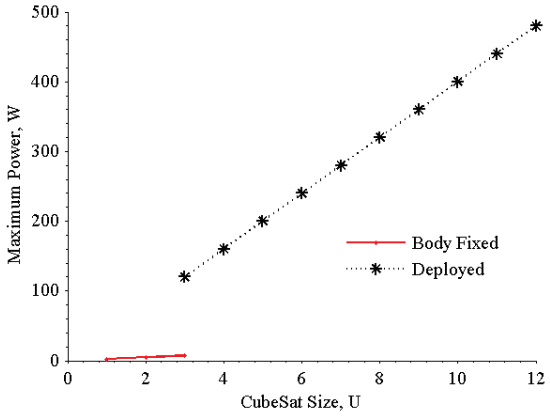

(a) Maximum Collected Power of Solar Panels

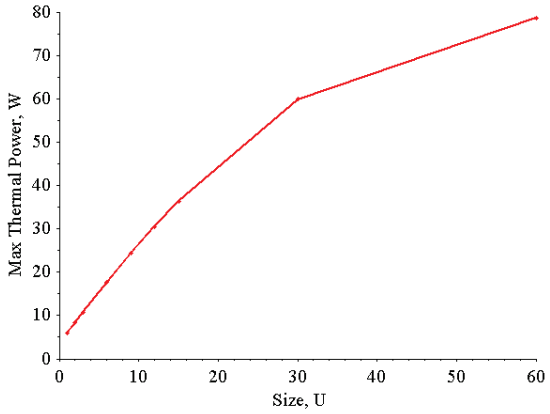

(b) Maximum Radiative Power of Radiator

Figure 2: Maximum Power scaling relationships for solar panels and radiator

Key thruster properties are plotted in Fig. 3. As expected, the maximum thrust to power declines with increase in I_{sp} in Fig. 3a for different thrusters. Most of the high thrust-to-power thrusters, such as the CAT Plasma, MIT iEPS, UCLA/JPL MiXI Ion, and Busek Ion (BIT-3) thrustrs are also relatively mass efficient, making them attractive for small spacecraft applications. Note this mass does not account for the propellant mass, which differs for the thrusters because of their different density propellants. This is addressed in the system-level analysis looking at realistic mission applications.

RESULTS

Performance Metrics

Space missions generally aim to maximize the capability of science instruments (in number or size), therefore the main goal in this problem is to maximize the mass margin, M_m. This can also be defined as

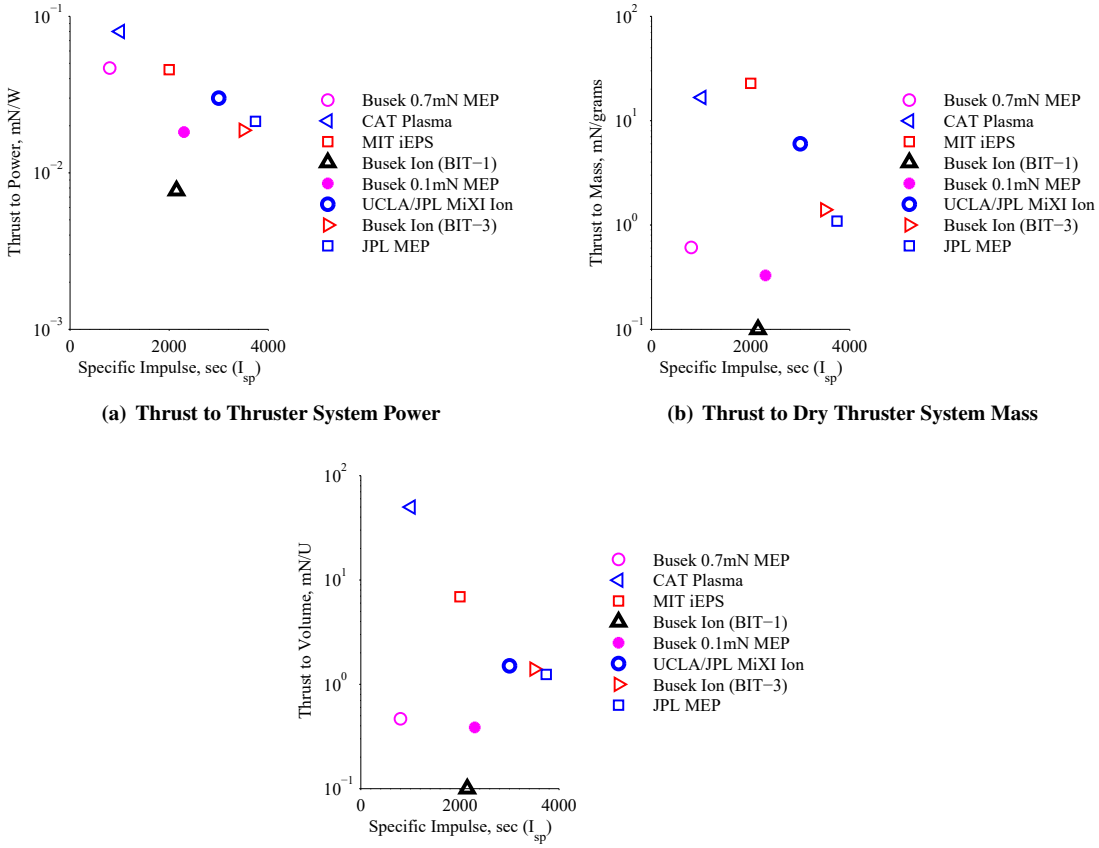

(a) Thrust to Thruster System Power

(b) Thrust to Dry Thruster System Mass

(c) Thrust to Dry Thruster System Volume

Figure 3: Key thruster properties for emerging small SEP technologies

Table 2: LEO and Deep Space Orbit Transfers Studied. All LEO orbits are circular and GEOs are equatorial.

Name	Initial Orbit	Final Orbit	ΔV range	Burn Time (days)	Time of Flight (days)
GTO to Lunar Flyby	GTO	Earth Escape	1.7-3.4 km/s	50-559	120-735
LEO to GEO	Equatorial, $a = 500$ km	GEO	4.4-5.5 km/s	77-658	178-917
ISS to Polar	$i = 52°$, $a = 420$ km	Polar, $a = 420$ km	6.7-7.6 km/s	82-543	121-553
ISS to Equatorial	$i = 52°$, $a = 500$ km	Equatorial, $a = 420$ km	9.3-11.3 km/s	85-711	123-735
Deimos Return	Deimos	Earth Orbit	5.5-9.6 km/s	18.4-738	272-756
Phobos Return	Phobos	Earth Orbit	6.3-10.4 km/s	22.5-868	276-886

the payload mass fraction, M_p/M_i, where M_p is the payload mass, including all spacecraft components not related to the propulsion system, and M_i is the initial wet spacecraft mass. We are also interested in solutions that minimize time of flight, T, particularly for small spacecraft that may have limited lifetimes due to both increased radiation exposure and thruster operating limits. Because these are often conflicting goals because higher I_{sp} values decrease M_m but increase T, we show Pareto fronts showing the trade-off between these goals in this section. Another approach could be to consider a set payload mass and design the propulsion system accordingly, which could reduce the overall propellant and time of flight times if the final spacecraft mass is lower than the maximum allowable mass.

Representative Missions

First we consider a simple constant thrusting maneuver for a specified ΔV value, where we assume these

missions operate in LEO, using the lower-mass radio described earlier. These examples are selected because it reduces the dimensionality of the problem because there are not multiple approaches to accomplish the mission. Furthermore it provides a fair way to compare the thrusters as there are no minimum thrust requirements, which is true for some of the upcoming examples.

Several representative mission scenarios are summarized in Table 2 from earlier work [11]. These are mission opportunities driven by science or exploration goals that are feasible with small spacecraft and determined based on input from JPL scientists and engineers. The orbital transfer ΔV, burn time, and transfer times span ranges as we considered a large solution space with diverse I_{sp} values.

Simple Maneuver Constant Thrusting Maneuver

The Pareto-fronts for this maneuver in Fig. 4, where the plot trends are nearly identical for maneuvers between ΔV=1 km/sec to 10 km/sec, however the curve shifts to lower mass margins and greater time of flights for larger ΔV requirements. The ΔV=7 km/sec is shown as it represents a significant orbital change, such as an orbital transfer from LEO to Earth escape for a 3U CubeSat [2] or a transfer from an International Space Station (ISS) to a polar orbit, see Table 2.
For a 6U spacecraft, as in Figs. 4b-4f, the Pareto fronts are quite clear in these plots, defined as connecting the CAT Plasma, MIT iEPS, UCLA/JPL MiXI, and JPL MEP thrusters (curve connecting the points that minimize flight time and maximize mass margin). As expected the thrusters are listed in increasing I_{sp} (1010, 2000, 3000, 3744 sec), which is correlated to longer T and larger M_m values. These thrusters dominate this curve as they also have high thrust-to-power and thrust-to-mass ratios, as in Fig. 3. For a 3U spacecraft, the Pareto front is less clear, and largely dominated by the Note the results are similar for larger spacecraft, but shifter to higher values, for example for a 12U the mass margins are shifted approximately 7-8$\%$ higher.

Complex Mission Scenarios

Next we consider more complex mission scenarios where there are multiple approaches to accomplish the mission with different I_{sp} and thrust values. In particular, we study the LEO to GEO transfer and LEO GTO to Lunary Flyby cases summarized in Table 2. The results for 3U, 6U, and 12U spacecraft are provided in Fig. 5 There is a 20-30$\%$ reduction in mass margin between the GTO to Lunar Flyby and LEO to GEO cases due to the change in ΔV. Shorter flight times are observed in the LEO to GEO case because the orbit transfer can be done immediately in some cases, while the GTO to Lunar Flyby often requires several long-duration orbtial periods to achieve the desired phasing and thrusting at perigee approach.

For 3U spacecraft, the CAT Plasma and MIT iEPS thrusters perform nearly identically and dominate the Pareto front. In this application, the differences in I_{sp} are offset by the ability to fly the fractional number of required thrusters to achieve the thrust level in every data point. The UCLA/JPL MiXI thruster also appears on the Pareto front for mid to high flight times. For 6U and 12U spacecraft, the CAT Plasma thruster outperforms the MIT iEPS thruster, likely due to the elimination of the power and thermal constrains limiting its performance. The MIT iEPS does dominate the Pareto front for high thrust times for the LEO to GTO maneuver, see Fig. 5e. Overall these results demonstrate that the optimal thruster for a given application is highly dependent on the mission and constraints (i.e. spacecraft size).

CONCLUSIONS

This paper has presented a modeling framework to enable the comparison of emerging electric propulsion thrusters for small spacecraft. We've developed an approach to integrate the trajectory and vehicle design to enable broad solution-space exploration and evaluation of key performance trade-offs. The results provide useful data for mission planners and architects to extract the best thruster for their application and set of constraints.

The key limiting factors for all thrusters was the thermal system, which generally limited the operating power of the propulsion system, particularly small spacecraft with limited surface area. This motivates the design of improved thermal systems that are not limited by the radiator surface area, for example those that use deployed radiators coupled with pumped fluid loops or freezable radiators.

Overall, we've noted the strong correlation high thrust-to-power and thrust-to-mass thrusters and dominating the Pareto trade-off between high payload mass fractions and low transfer times. The CAT Plasma, MIT iEPS, UCLA/JPL MiXI, and JPL MEP thrusters created the Pareto front for the simple constant thruster manevuers, while the CAT Plasma and MIT iEPS thrusters dominated the Pareto fronts for more complex but relatively low ΔV maneuvers. We expect the UCLA/JPL MiXI and JPL MEP thrusters may perform best for higher ΔV and longer-duration orbit transfers due to their high I_{sp} values. It is clear there are applications where thrusters spanning the range of I_{sp} values presented here are op-

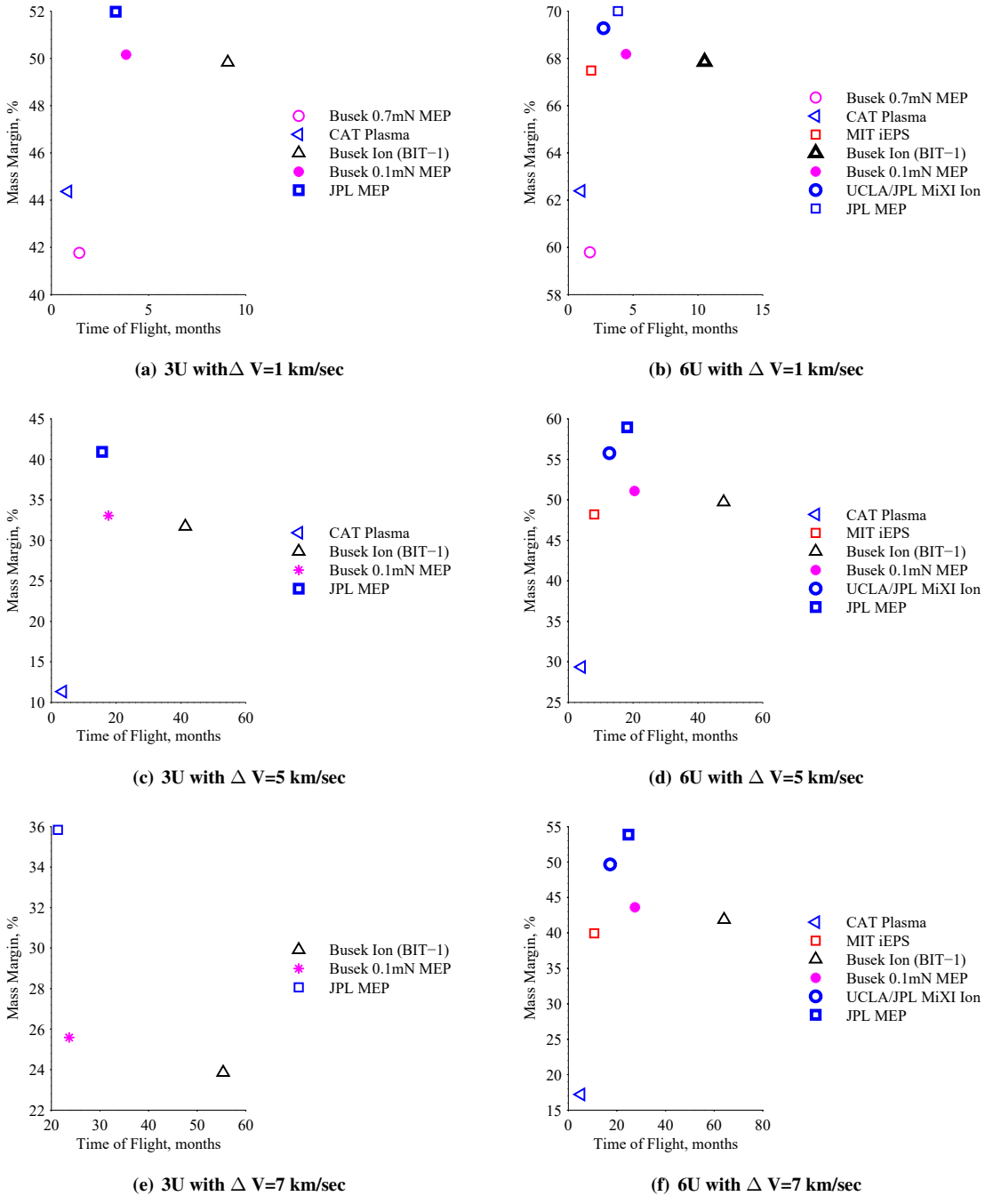

(a) 3U with△ V=1 km/sec

(b) 6U with △ V=1 km/sec

(c) 3U with △ V=5 km/sec

(d) 6U with △ V=5 km/sec

(e) 3U with △ V=7 km/sec

(f) 6U with △ V=7 km/sec

Figure 4: Pareto trade-off between mass fraction and maneuver duration for constant thrusting case for a 3U and 6U CubeSat.

timal. Based on these results, continued development of all thrusters along the Pareto front are highly encouraged, as well as others that have a high potential of similar performance.

ACKNOWLEDGMENTS

The author acknowledges Colleen Marrese-Reading, Thomas Randolf, Damon Landau, Shawn Johnson, Nitin Aurora, John Ziemer, Julie Catillo-Rogez and Andrew Gray for their contributions. Part of the research was

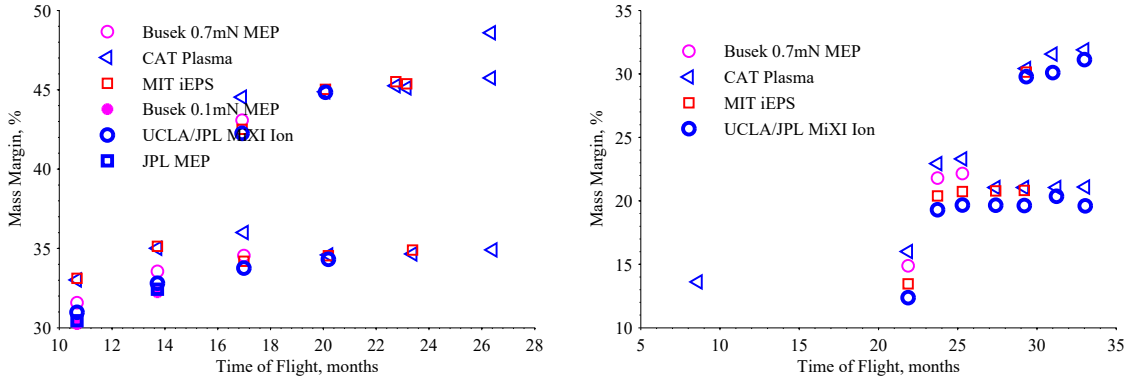

(a) 3U LEO GTO to Lunar Flyby ($\Delta V = 1.7 - 3.4$ km/sec) **(b) 3U LEO to GEO ($\Delta V = 4.4 - 5.5$ km/sec)**

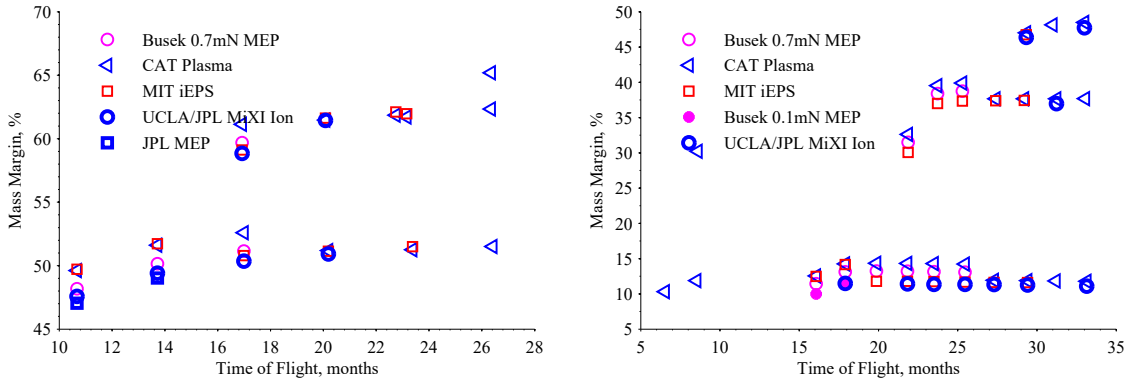

(c) 6U LEO GTO to Lunar Flyby ($\Delta V = 1.7 - 3.4$ km/sec) **(d) 6U LEO to GEO ($\Delta V = 4.4 - 5.5$ km/sec)**

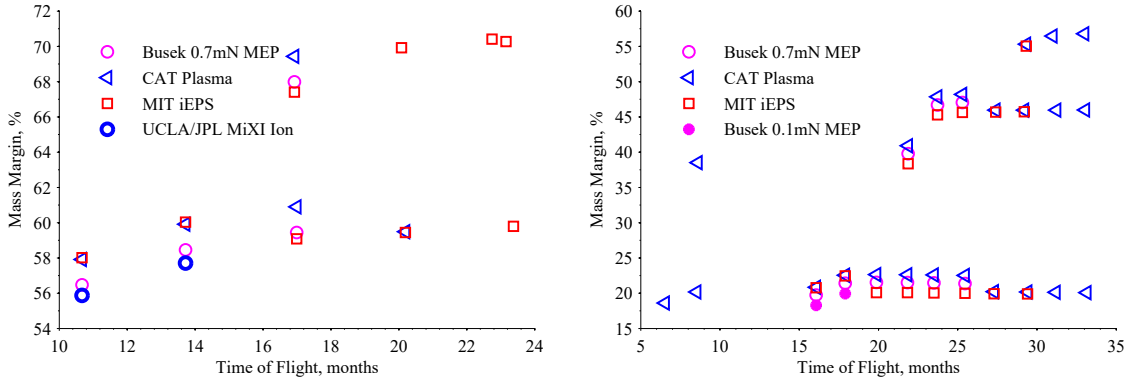

(e) 12U LEO GTO to Lunar Flyby ($\Delta V = 1.7 - 3.4$ km/sec) **(f) 12U LEO to GEO ($\Delta V = 4.4 - 5.5$ km/sec)**

Figure 5: Pareto fronts for LEO transfer orbits and different spacecraft sizes (3U, 6U, and 12 U).

carried out at the Jet Propulsion Laboratory, California Institute of Technology, under a contract with the National Aeronautics and Space Administration.

REFERENCES

1. Mueller, J., H. R. and Ziemer, J., "Survey of propulsion technologies applicable to cubesats," *Proceedings of the 57th Joint Army-Navy-NASA-Air Force (JANNAF) Propulsion Meeting*, Colorado Springs, CO, 2010.
2. Sara Spangelo, Julie Castillo-Rogez, A. F. A. K. B. S., "JPLs Advanced Interplanetary CubeSat Concepts for Science and Technology Demonstrations," *Interplanetary Small Satellite Conference*, Santa Clara, CA, 2015.
3. Rayman, M. D. and Williams, S. N., "Design of the First

Interplanetary Solar Electric Propulsion Mission," *Journal of Spacecraft and Rockets*, Vol. 39, No. 4, 2002, pp. 589–595.
4. Steven N. Williams, V. C.-C., "Mars Missions Using Solar Electric Propulsion," *Journal of Spacecraft and Rockets*, Vol. 37, No. 1, 2000, pp. 71–77.
5. Oh, D. Y., "Evaluation of Solar Electric Propulsion Technologies for Discovery-Class Missions," *Journal of Spacecraft and Rockets*, Vol. 44, No. 2, 2007, pp. 399–411.
6. L. E. Schwaiger, J. M. Schollenberger Jr., J. H. M. and MacPherson, D., "Solar Electric Propulsion Asteroid Belt Mission," *Journal of Spacecraft and Rockets*, Vol. 8, No. 6, 1971, pp. 612–617.
7. J. Wang, D. E. Brinza, D. T. Y. J. E. N. J. E. P. M. D. H. R. G. J. J. H. D. J. L. M. S., "Deep Space One Investigations of Ion Propulsion Plasma Environment," *Journal of Spacecraft and Rockets*, Vol. 37, No. 5, 2000, pp. 545–555.
8. John Steven Snyder, Thomas M. Randolph, R. R. H. D. M. G., "Simplified Ion Thruster Xenon Feed System For NASA Science Missions," *31st International Electric Propulsion Conference*, Ann Arbor, MI, 2009.
9. Co, T. C. and Black, J. T., "Responsiveness in Low Orbits Using Electric Propulsion," *Journal of Spacecraft and Rockets*, Vol. 51, No. 3, 2014, pp. 938–945.
10. Sara Spangelo, D. D. and Longmier, B., "Small Spacecraft System-level Design and Optimization for Interplanetary Trajectories," *Journal of Spacecraft and Rockets*, May 2015.
11. Sara Spangelo, Damon Landau, S. J. N. A. T. R., "Defining the Requirements for the Micro Electric Propulsion Systems for Small Spacecraft Missions," *Proceedings of the IEEE Aerospace Conference*, Big Sky, MT, March 2005.
12. Conversano, R. and Wirz, R., "CubeSat Lunar Mission Using a Miniature Ion Thruster," *47th AIAA/ASME/SAE/ASEE Joint Propulsion Conference and Exhibit*, San Diego, CA, July 2011.
13. (BCT), B. C. T., "XB1: High Performance 1U CubeSat Bus Specification Sheet," BCT Website, 2014.